Brownian motion on a square Lennard-Jones lattice: Trapping, hopping, and diffusion

Li-Shi Luo* and George D. J. Phillies
Department of Physics, Worcester Polytechnic Institute, Worcester, Massachusetts 01609-2280

Louis Colonna-Romano and Harvey Gould
Department of Physics, Clark University, Worcester, Massachusetts 01610

(Received 26 May 1994)

We studied the Brownian motion of a single probe particle moving through a square array of fixed lattice particles. Brownian motion was simulated via the dynamic Metropolis algorithm. The probe-lattice particle interaction was the Lennard-Jones potential. In addition to the mean-square displacement and effective diffusion coefficient studied by previous workers, we obtained such diagnostics as the two-point density of states $\rho^{(2)}(\delta\mathbf{r})$, its angular average $\rho^{2}(\delta r)$, the correlation function $P(\delta r,\tau)$ for distances δr traveled by probe particles during the elapsed time τ, and the probe dynamic structure function $S(\mathbf{k},\tau)$. By varying the temperature and density, we observed distinct diffusive, hopping, and trapping regimes; our computed diagnostics of system behavior reflect different aspects of these regimes in a mutually consistent way.

PACS number(s): 05.40.+j, 66.30.Hs, 83.20.Jp

I. INTRODUCTION

The diffusion of small probe particles through a complex background is a recurring theme in the study of complex materials, including observations on polymer chains in fumed silica [1] and Vycor glasses [2] saturated with solvent, methane and other small molecules in polymer matrices [3], polystyrene spheres and other probes in polyacrylamide and related gels [4–11], and noble gas and similar molecules in pillared clays [12]. Experimental techniques for measuring probe diffusion include gravimetric analysis [12], quasielastic light scattering [4], forced Rayleigh scattering [1], and fluorescence recovery after photobleaching [13]. The dependence of probe diffusion on temperature and matrix structure and density has been studied extensively.

These experimental data have been compared with a variety of computer simulations using molecular dynamics and Monte Carlo methods. For example, Chen *et al.* [12] considered an on-lattice computation on a triangular lattice on which some lattice lines are permanently open and others, chosen randomly, are permanently closed. Müller-Plathe [3] reported a molecular dynamics simulation of a small object (a gas molecule) diffusing through a high density of potentially mobile model polyethylene chains. In each case a probe trajectory was computed and subjected to statistical analysis. Calculated quantities included $\langle[\delta\mathbf{r}(\tau)]^2\rangle$, the mean-square displacement of single probe particles as a function of the elapsed time τ, and the effective diffusion coefficient $\bar{D}$.

Here we report results from our simulations of probe diffusion through a two-dimensional matrix of lattice points. The probe interacts with the lattice points via a Lennard-Jones potential. Because we studied a regular lattice, nonergodic behavior due to local irregularities in the particle density or placement is excluded. An important advantage of computer simulations is that they permit the measurement of quantities that are not readily accessible experimentally. In addition to the mean-square displacement and the effective diffusion coefficient measured in previous simulations [3,12], we report results for the two-point density of states $\rho^{(2)}(\delta\mathbf{r})$, its angular average $\rho^{(2)}(\delta r)$, the probability density $P(\delta r,\tau)$ for distances δr traveled by probe particles during the elapsed time τ, and the probe dynamic structure function $S(\mathbf{k},\tau)$. We obtain different types of probe behavior, including trapping, hopping, and diffusion, by varying the temperature of the probe particle and the density of the lattice. A variety of computed diagnostics are shown to reveal different aspects of these behaviors in a self-consistent way.

II. COMPUTATIONAL METHODS

Our system is a square lattice containing 100×100 lattice points, with periodic boundary conditions imposed. A rigidly fixed Lennard-Jones particle is placed on each lattice point. The lattice spacing is $a=1/\sqrt{\rho}$, where ρ is the lattice point density. We study a single probe particle diffusing off-lattice in the spaces between the lattice particles. The probe particle interacts with the lattice points by the Lennard-Jones 12-6 potential

$$u(\mathbf{r})=\left[\frac{\sigma}{r}\right]^{12}-\left[\frac{\sigma}{r}\right]^{6}, \tag{1}$$

where $\sigma=\frac{1}{2}(\sigma_0+\sigma_1)$. The probe and lattice radii σ_0 and

*Present address: MS-B213, Complex Systems Group T-13, Theoretical Division, Los Alamos National Laboratory, Los Alamos, New Mexico 87545.

σ_1 are 0.1 and 1.0, respectively, in arbitrary distance units so that $\sigma=0.55$. In our simulations, we choose a cutoff interaction radius $r_{\max}=10.5\sigma$. The total potential energy $U(\mathbf{r})$ of the probe is computed ignoring the lattice particles that are more than $r_{\max}$ away from the probe.

The probe particle dynamics is based on the Metropolis algorithm [15]. We generate random steps of maximum length r_0. The probability that a random step is accepted is $\exp[-\beta\Delta U(\mathbf{r})]$, where $\beta=1/k_BT$, T is the temperature, and ΔU is the change in the potential energy between the beginning and the end of the step. To ensure the isotropy of the random walk, we separately generate step components δx and δy along the x and y axes, rejecting steps that do not satisfy the condition

$$\delta x^2+\delta y^2\le r_0^2 \ . \tag{2}$$

The step components δx and δy are chosen from a uniformly distributed (pseudo)random variable. Over small numbers of steps and very short distances, the random walk has a non-Gaussian distribution of displacements; the central theorem guarantees that the displacement distribution converges (swiftly in this case) to a diffusive ($\delta x^2,\delta y^2\sim N^1$, N being the number of steps) distribution. Our Monte Carlo simulations were done for a series of values of the lattice density ρ and temperature T.

We compute the mean-square displacement of single probe particles as a function of the time displacement τ

$$\langle[\delta\mathbf{r}(\tau)]^2\rangle=\langle\|\mathbf{r}(t+\tau)-\mathbf{r}(t)\|^2\rangle$$
$$=\frac{1}{N_0}\sum_{i=1}^{N_0}\|\mathbf{r}(t_i+\tau)-\mathbf{r}(t_i)\|^2 \tag{3}$$

by averaging Eq. (3) over the N_0 choices of the time origin t_i. The effective diffusion coefficient $\bar{D}$ is defined as

$$\bar{D}=\left\langle\frac{[\delta\mathbf{r}(\tau)]^2}{4\tau}\right\rangle \tag{4}$$

by a weighted linear least squares fit using weight $1/\tau$. The determinations of $\langle[\delta\mathbf{r}(\tau)]^2\rangle$ always began with 5×10^5 Monte Carlo steps to thermalize the probe particle. We then did 2×10^6 samples of $[\delta\mathbf{r}(\tau)]^2$, $P(\delta r,\tau)$, and $S(\mathbf{k},\tau)$ with 200 Monte Carlo steps between each sample. All calculations were done on a DEC alpha computer workstation. The random number generators used in the simulations were RAN2( ) of Press *et al.* [14], and routine RANDOM( ) in the DEC workstation FORTRAN library.

We also compute the probe dynamic structure function

$$S(\mathbf{k},\tau)=\langle e^{i\mathbf{k}\cdot[\mathbf{r}(t+\tau)-\mathbf{r}(t)]}\rangle$$
$$\equiv\int dt\, e^{i\mathbf{k}\cdot[\mathbf{r}(t+\tau)-\mathbf{r}(t)]} \ , \tag{5}$$

and the distribution function $P(\delta r,\tau)$. The two-point density of states

$$\rho^{(2)}(\delta\mathbf{r})=\frac{\int e^{-\beta U(\delta\mathbf{r}+\mathbf{r}')}e^{-\beta U(\mathbf{r}')}d\mathbf{r}'}{\int e^{-\beta U(\mathbf{r}')}d\mathbf{r}'} \tag{6}$$

gives the uncorrelated average joint probability of finding a particle at two points separated by $\delta\mathbf{r}$. $\rho^{(2)}(\delta\mathbf{r})$ was computed by numerical integration. The angular average $\rho^{(2)}(\delta r)$ of $\rho^{(2)}(\delta\mathbf{r})$, used in the following to interpret $P(\delta r,\tau)$, was obtained by a Monte Carlo integration from $\exp[-\beta U(\mathbf{r})]$, not by a direct integration of $\rho^{(2)}(\delta\mathbf{r})$.

III. NUMERICAL RESULTS AND DISCUSSION

In the following, we present numerical results for three distinct types of probe behavior, namely, trapping, hopping, and diffusion. This behavior can be observed by varying the temperature T for a fixed lattice density ρ. As the temperature rises, a transition from trapping to hopping and from hopping to diffusion occurs. We also identified a second high density, low temperature regime in which the particles should be trapped in a region of space different from the region in which trapping occurs at low densities.

The functions of interest are the mean-square displacement $\langle[\delta\mathbf{r}(\tau)]^2\rangle$ of the probe particle as a function of time τ, the effective diffusion coefficient $\bar{D}$, the probability function $P(\delta r,\tau)$, the two-point density of states $\rho^{(2)}(\delta\mathbf{r})$ and its angular average $\rho^{(2)}(\delta r)$, the ratio $P(\delta r,\tau)/\rho^{(2)}(\delta r)$, and the dynamic structure function of the probe $S(\mathbf{k},\tau)$.

$\bar{D}$ is conveniently normalized by D_0, the diffusion coefficient of the probe particle in free space. D_0 is obtained from the two-dimensional mean-square displacement $\langle\mathbf{r}^2\rangle$ during t via $\langle\mathbf{r}^2\rangle=4D_0t$. For a random walker with independent steps, $\langle\mathbf{r}^2\rangle$ for N steps is N-fold larger than $\langle\mathbf{r}^2\rangle$ for a single step. D_0 for a random walker at large times can therefore be computed from $\langle\mathbf{r}^2\rangle$ for a single step, even if the small steps do not have a Gaussian probability distribution. In particular, for steps having a uniform distribution on a disc of radius r_0, D_0 is given by

$$D_0=\frac{1}{4}\frac{\int_0^{r_0}\mathbf{r}^2d\mathbf{r}}{\int_0^{r_0}d\mathbf{r}}=\tfrac{1}{8}r_0^2 \ . \tag{7}$$

The behavior of a probe is determined by the shape of the potential energy surface. Figure 1 shows the total potential energy surfaces for the lattice density $\rho=0.09$, 0.64, and 0.81. Because the total potential energy $U(\mathbf{r})$ has the periodicity and rotational symmetry of the underlying lattice structure, all the features of the complete potential energy surface appear in one fourth of a unit cell. The lattice particles are fixed and $U(\mathbf{r})$ as experienced by the probe varies only because the probe samples different values of $\mathbf{r}$.

At the lowest lattice density [Fig. 1(a)], $U(\mathbf{r})$ is dominated by the nearby lattice point at the origin; contributions to $U(\mathbf{r})$ from other lattice points are small because the lattice spacing a is large relative to σ. $U(\mathbf{r})$ has a high, steep central repulsive core, surrounded by a circularly symmetric deep minimum due to the attractive r^{-6} part of the Lennard-Jones potential. At the higher density $\rho=0.64$ [see Fig. 1(b)], a local maximum appears at the center of the lattice cell in addition to the repulsive central core; a localized minimum is found midway between neighboring lattice points along a lattice line. At the

highest density considered [$\rho=0.81$, Fig. 1(c)], the potential energy minima move off the lattice lines toward the cell center, with minima approximately at ($0.25a$, $0.5a$) and ($0.5a$, $0.25a$). These minima are isolated; to cross a lattice grid line from one minimum to the next, it is necessary to cross a local saddle point in the potential energy.

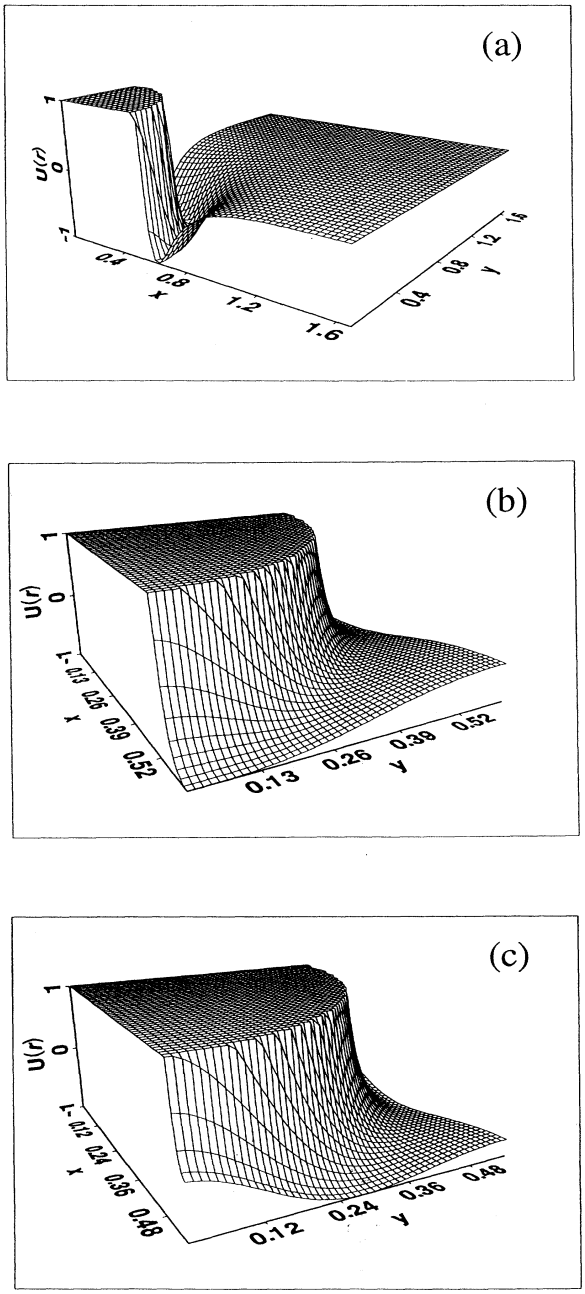

FIG. 1. Total probe-lattice potential energy $U(\mathbf{r})$ for lattice densities ρ of (a) 0.09, (b) 0.64, and (c) 0.81. $U(\mathbf{r})$ is normalized so that its minimum is -1. A lattice particle is at the origin; the figure shows $\frac{1}{4}$ of a unit cell.

A. Mean-square displacement

Figure 2 shows $\langle[\delta\mathbf{r}(\tau)]^2\rangle$ as a function of time and illustrates the three characteristic types of behavior of the probe particle. The parameters are $\rho=0.09$ and $r_0=0.025$. At the lowest temperature [$k_BT=0.01$, Fig. 2(a)], the probe is trapped. For a trapped probe the displacement $\langle[\delta\mathbf{r}(\tau)]^2\rangle$ first increases while the probe explores the circular potential energy minimum [see Fig. 1(a)], but ceases to increase once the probe has explored the accessible part of its space. At an intermediate temperature ($k_BT=0.02$), the probe shows hopping behavior, and is trapped on short time scales, but moves freely on longer time scales. At this temperature, $\langle[\delta\mathbf{r}(\tau)]^2\rangle$ has a plateau for $2\times10^4\leq\tau\leq2\times10^6$; at $\tau>2\times10^6$ $\langle[\delta\mathbf{r}(\tau)]^2\rangle$ increases without bound. At high

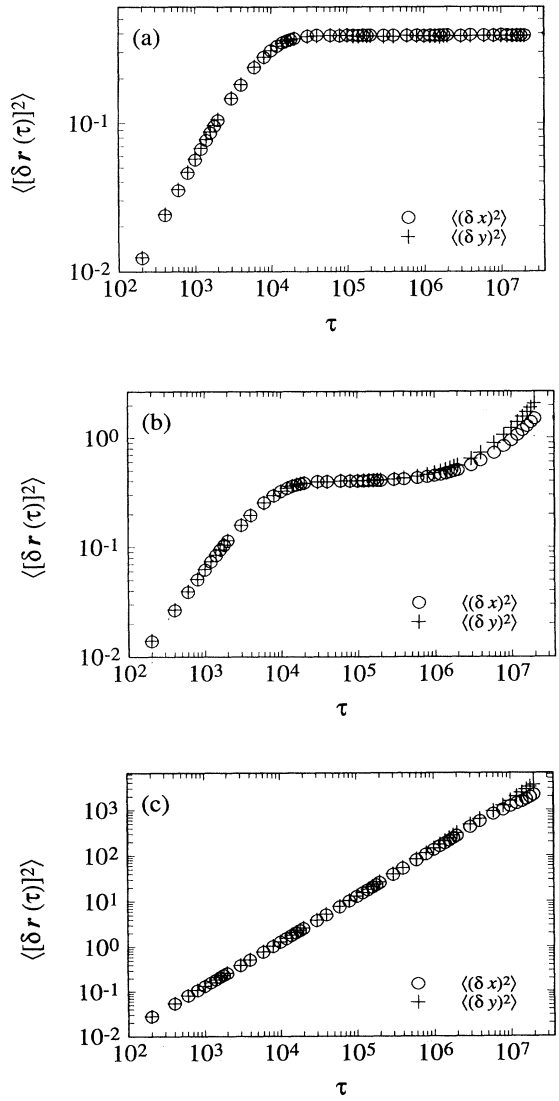

FIG. 2. Mean-square displacement $\langle[\delta\mathbf{r}]^2\rangle$ as a function of the time τ with $\rho=0.09$ at temperature k_BT of (a) 0.01 (trapping behavior), (b) 0.02 (hopping behavior), and (c) 0.1 (diffusive behavior).

temperature ($k_BT=0.1$), the probe diffuses freely, with no indication of hopping behavior; the mean-square probe displacement $\langle[\delta\mathbf{r}(\tau)]^2\rangle$ increases uniformly on all time scales.

The distinction between trapping and hopping behavior arises purely from the time scale of observation. If the probe had been observed only at time intervals $\tau<10^6$ for $k_BT=0.02$, the probe would have appeared to be trapped, with $\langle[\delta\mathbf{r}(\tau)]^2\rangle$ becoming constant. Similarly, at $k_BT=0.01$, it is reasonable to suppose—at time scales longer than those considered here—the probe would eventually have escaped and shown hopping behavior.

In the limit of large sample counts, the symmetry of our potential energy guarantees that motions along the x and y axes should show precisely the same behavior. This requirement is not always precisely satisfied by our data. There are two effects here. First, our longest delay times are not arbitrarily shorter than the total length of a simulation. At the longest delay times that we report, the number of independent samples of $[\delta\mathbf{r}(\tau)]^2$ is relatively small, so our determination of $\langle[\delta\mathbf{r}(\tau)]^2\rangle$ becomes increasingly noisy at large τ. Second, in the hopping regime, as the system becomes colder and colder, the interval between hops becomes longer and longer. As a result, no matter how long a simulation is performed, there will always be temperatures at which only a few hops occur during a single computer run; at these temperatures, the noisy statistics of small numbers will typically cause $\langle[x(\tau)]^2\rangle$ and $\langle[y(\tau)]^2\rangle$ to differ from each other.

Figure 3 and Table I give $\bar{D}/D_0$ as a function of T at values of ρ. Table I also gives the percent standard deviations of $\bar{D}/D_0$. If the probe remains trapped on the time scale of our simulations, we can infer only an upper bound (not necessarily a least upper bound) for $\bar{D}/D_0$; in these cases we give no error estimate. Figure 3 indicates

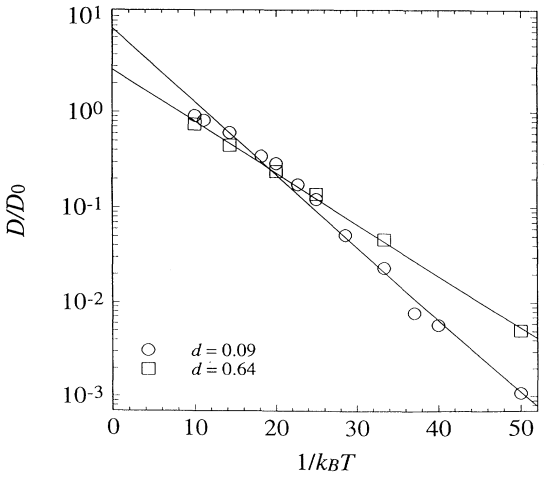

FIG. 3. Effective diffusion coefficient $\bar{D}/D_0$ versus k_BT at densities 0.09 (○) and 0.64 (□). Straight lines are least squares fits of data to an Arrhenius form, indicating Arrhenius activation energies of 0.176 ± 0.0006 ($\rho=0.09$) and 0.125 ± 0.0009 ($\rho=0.64$).

TABLE I. The effective diffusion coefficient $\bar{D}/D_0$ as a function of the temperature T at lattice densities of $\rho=0.09$ and 0.64.

	$\bar{D}/D_0$	
k_BT	$\rho=0.09$	$\rho=0.64$
0.005	6×10^{-5}	6×10^{-7}
0.01	6×10^{-5}	4×10^{-6}
0.012		1×10^{-5}
0.015		2×10^{-4}
0.02	$1.1\times10^{-3}\pm53.5\%$	$5.1\times10^{-3}\pm11.6\%$
0.025	$5.8\times10^{-3}\pm11.8\%$	
0.027	$5.1\times10^{-2}\pm7.44\%$	
0.03	$2.32\times10^{-2}\pm2.48\%$	$4.61\times10^{-2}\pm1.28\%$
0.035	$5.14\times10^{-2}\pm1.30\%$	
0.04	$0.1215\pm0.47\%$	$0.1373\pm0.42\%$
0.044	$0.1732\pm0.33\%$	
0.05	$0.2886\pm0.21\%$	$0.2390\pm0.24\%$
0.055	$0.3449\pm0.167\%$	
0.07	$0.6090\pm0.098\%$	$0.4471\pm0.15\%$
0.09	$0.8164\pm0.072\%$	
0.1	$0.9112\pm0.066\%$	$0.7414\pm0.078\%$

that the temperature dependence of $\bar{D}/D_0$ approximately follows an Arrhenius type relation,

$$\frac{\bar{D}}{D_0}=e^{-E_A/k_BT}, \tag{8}$$

at both densities studied. The activation energy E_A is nearly independent of temperature at both densities. Least squares fits to the data in Table I yield 0.1759 ± 0.0006 ($\rho=0.09$), and 0.1245 ± 0.0009 ($\rho=0.64$) for E_A.

B. Time-dependent displacement distribution and the two-point density of states

Figure 4 shows the probability $P(\delta r,\tau)$ that a probe travels a distance δr in time τ for τ ranging from 200 to 2×10^7 steps, for a total run of 4×10^8 Monte Carlo steps. The temperatures given ($k_BT=0.01$, 0.02, and 0.1) correspond to trapping, hopping, and free diffusion.

Figure 4(a) shows trapping behavior. At short times, $P(\delta r,\tau)$ is nearly Gaussian. With increasing τ, $P(\delta r,\tau)$ becomes nonzero over wider and wider regions. However, in the cold system the probe particle is trapped in the potential energy minimum seen in Fig. 1(a). At long times (τ between 2×10^5 and 2×10^7 steps), the location of the probe has become uncorrelated with its initial position and $P(\delta r,\tau)$ becomes virtually independent of τ. The potential energy minimum has a diameter $2\sqrt[6]{2\sigma}$, so a thermalized probe never moves farther than $\delta r\approx1.5$ from its starting point. (A nonthermalized probe placed randomly on the lattice might initially move more than $\delta r\approx1.5$, but during the thermalization such a probe would become trapped in a potential energy minimum, so that at the start of the simulation the probe would be trapped).

Figure 4(b) shows hopping behavior. At very short times, $P(\delta r,\tau)$ is approximately Gaussian. At longer

times, the probe is trapped within a potential energy minimum, so $P(\delta r,\tau)$ shows an accumulation near $\delta r=1.5$ and falls nearly to zero at larger δr. At even longer times, the probe passes the barrier confining it to the region $\delta r<1.5$, and penetrates into the region $\delta r>2.0$. As $\tau\rightarrow 10^7$ steps, at fixed $\delta r>2.0$, $P(\delta r,\tau)$ increases monotonically over the observed τ. The fine structure in $P(\delta r,\tau)$ at $\delta r>2.0$ is discussed below.

At the highest temperature studied [Fig. 4(c)], the qualitative shape of $P(\delta r,\tau)$ changes little as time evolves. $P(\delta r,\tau)$ remains approximately Gaussian at all times, and the mean-square width of $P(\delta r,\tau)$ increases approximately monotonically with τ. The Gaussian behavior of $P(\delta r,\tau)$ for all times clearly indicates that the probe diffuses without trapping on any time scale.

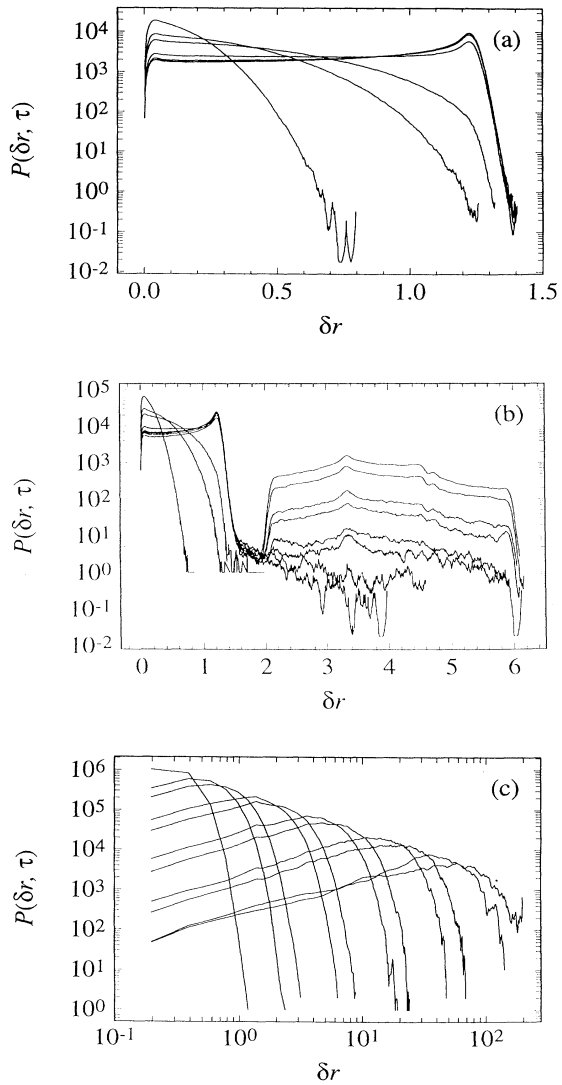

FIG. 4. Probability distribution $P(\delta r,\tau)$ at temperatures k_BT of (a) 0.01, (b) 0.02, and (c) 0.1. The curves connect points of fixed τ for $\tau=2\times10^2$, 10^3, 2×10^3, 10^4, 2×10^4, 10^5, 2×10^5, 10^6, 2×10^6, 10^7, and 2×10^7 Monte Carlo steps. In (a) the larger τ curves are not distinguishable. Some curves were smoothed by averaging over sets of 21 nearby points.

A generalized Vineyard approximation [16]

$$P(\delta r,\tau)=e^{-(\delta r)^2/4D\tau}\rho^{(2)}(\delta r) \tag{9}$$

describes diffusion through an irregular potential energy surface in terms of a diffusive process and a surface whose statistical weight in coordinate space is a function of position. The two-point density of states $\rho^{(2)}(\delta r)$ gives the uncorrelated average joint probability for finding particles at two points separated by δr. For a system with periodic boundary conditions, thermal equilibrium requires that $P(\delta r,\tau)$ should go to $\rho^{(2)}(\delta r)$ at large τ. Equation (9) is a mean-field approximation, in which it is assumed that the background potential renormalizes D, but that the detailed structure of $U(\mathbf{r})$ does not influence the details of the dispersion of δr at intermediate τ.

Figures 5(a) and 5(b) show $\rho^{(2)}(\delta\mathbf{r})$ for a relatively low density ($\rho=0.09$) at temperatures $k_BT=0.02$ and 0.1. $\rho^{(2)}(\delta\mathbf{r})$ has the periodicity and symmetry of the lattice structure; we therefore only need to show $\rho^{(2)}(\delta\mathbf{r})$ over $\frac{1}{4}$ of a unit cell. At both temperatures $\rho^{(2)}(\delta\mathbf{r})$ shows a central maximum and an annular local maximum centered on the origin. At $k_BT=0.02$, $\rho^{(2)}(\delta\mathbf{r})$ is nearly zero beyond the local maximum, while at $k_BT=0.1$, $\rho^{(2)}(\delta\mathbf{r})$ is substantially positive throughout all space.

The central maximum of $\rho^{(2)}(\delta\mathbf{r})$ arises because a thermalized probe is usually initially in a potential energy minimum, and small displacements leave the probe in the same potential energy minimum. The circular maximum in $\rho^{(2)}(\delta\mathbf{r})$ indirectly corresponds to the annular potential energy minimum seen in Fig. 1(a). $\rho^{(2)}(\delta\mathbf{r})$ is dominated by the contribution of pairs of points, both of which are in the circular potential energy minimum. The number of such pairs of points has a local maximum for pairs of points located nearly on opposite sides of the annulus covering the potential energy minimum, so $\rho^{(2)}(\delta\mathbf{r})$ has a circular maximum whose radius is twice the radius of the annular minimum of $U(\mathbf{r})$.

Figures 5(c) and 5(d) show $\rho^{(2)}(\delta\mathbf{r})$ for a relatively high density ($\rho=0.64$) and temperatures k_BT of 0.02 and 0.1. At the high density, the lattice spacing a is approximately half the radius of the single particle potential energy minimum, so a significant number of particles contribute appreciably to $U(\mathbf{r})$ at each $\mathbf{r}$. Besides the high central core, $\rho^{(2)}(\delta\mathbf{r})$ has features corresponding to the structure of the underlying lattice: ridges along lattice lines and a local maximum in the center of the lattice cell. These features are due to the overlap of potential energy minima from nearby lattice points. At low temperature and high density, $\rho^{(2)}(\delta\mathbf{r})$ is zero over broad areas, implying hopping or trapping behavior; at higher temperatures, $\rho^{(2)}(\delta\mathbf{r})$ is appreciably nonzero over most of its range, implying diffusive behavior.

Further analysis of $P(\delta r,\tau)$ is based on the angular average $\rho^{(2)}(\delta r)$ of $\rho^{(2)}(\delta\mathbf{r})$; Fig. 6 shows the latter function for the density $\rho=0.09$ and temperatures $k_BT=0.01$, 0.02, and 0.1.

We applied an inverted Vineyard approximation as a diagnostic for trapping. We consider a function

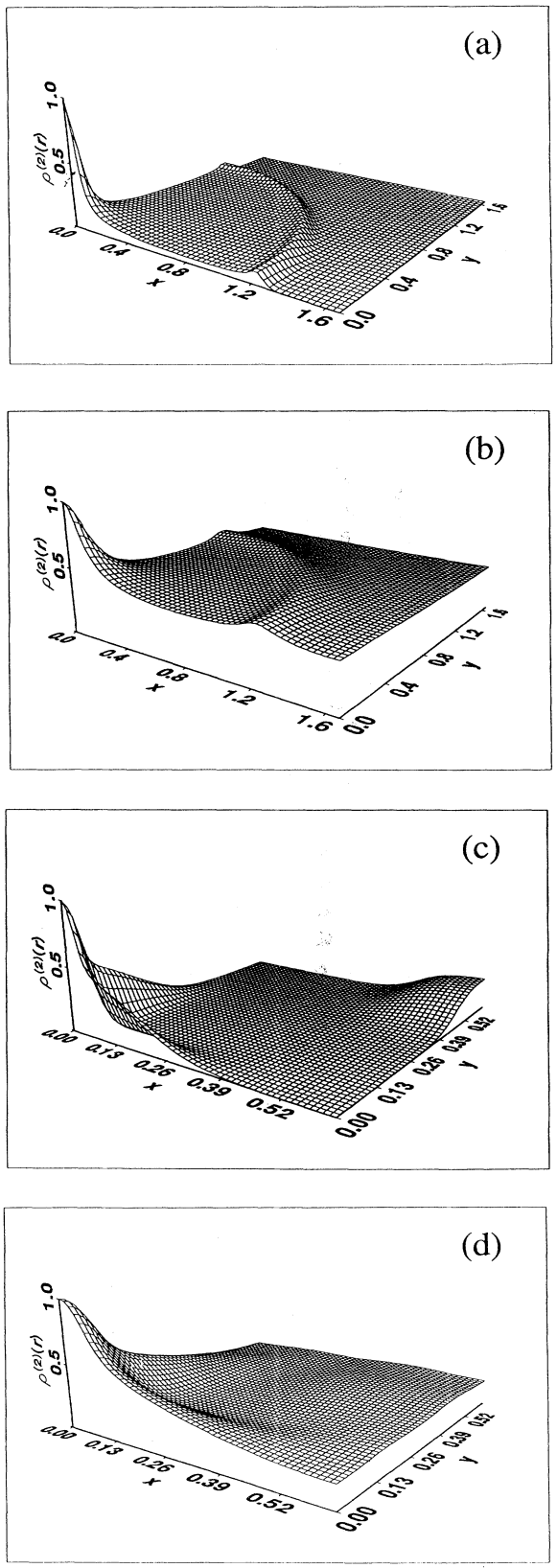

FIG. 5. Two-point density of states $\rho^{(2)}(\delta \mathbf{r})$ at $\rho=0.09$ and (a) $k_B T=0.02$, (b) $k_B T=0.1$, and $\rho=0.64$ and (c) $k_B T=0.02$, (d) $k_B T=0.1$.

$$\Psi(\delta r,\tau)=\frac{P(\delta r,\tau)}{\rho^{(2)}(\delta r)} \ . \tag{10}$$

$\Psi(\delta r,\tau)$ characterizes the spatiotemporal dispersion of the probe with purely static effects divided out. Figure 7 shows $\Psi(\delta r,\tau)$ at low density ($\rho=0.09$) and temperatures in the trapping, hopping, and diffusive regimes ($k_B T=0.01$, 0.02, and 0.1, respectively).

Figure 7(a) shows low temperature trapping behavior. For very short times (less than 2000 Monte Carlo steps) $\Psi(\delta r,\tau)$ appears to be Gaussian. At times $\tau \geq 10^5$ steps, trapping becomes visible, with $\Psi(\delta r,\tau)$ increasing as δr for small δr due to the Jacobian converting Cartesian to polar coordinates, but remaining approximately zero for $\delta r \geq 1.5$. Figure 7(b) shows how the potential energy surface correlates with hopping behavior. As may be seen by comparing Figs. 7(a) and 7(b) within the trap ($\delta r < 1.5$), $\Psi(\delta r,\tau)$ is no different for a hopping than for

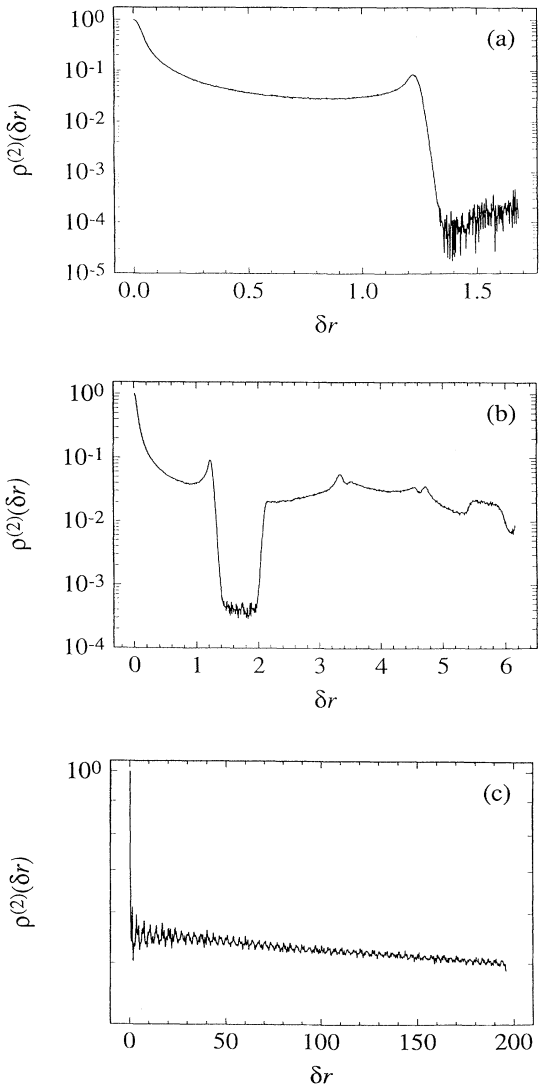

FIG. 6. Angular average $\rho^{(2)}(\delta r)$ of the two-point density of states at $\rho=0.09$ and temperatures $k_B T$ of (a) 0.01, (b) 0.02, and (c) 0.1.

a trapped particle. The barrier occupies $1.5 \leq \delta r \leq 2.0$. Compare Figs. 4(b) and 7(b); the very deep barrier minimum seen in Fig. 4(b) [$P(\delta r,\tau)$ is depressed by approximately three orders of magnitude within the barrier] disappears in Fig. 7(b), showing that the minimum is purely a density of states effect that is eliminated if the two-point density of states is divided out. Beyond the barrier ($\delta r > 2.0$), $\Psi(\delta r,\tau)$ at fixed δr grows monotonically in time, clearly showing hopping by the probe. Finally, at the highest temperature studied [Fig. 7(c)], $\Psi(\delta r,\tau)$ remains approximately Gaussian at all times, corresponding to diffusive motion, with no indication of a significant barrier effect on any time scale.

C. Dynamic structure function

Light scattering spectroscopy and inelastic neutron scattering measure not $P(\delta r,\tau)$ but its spatial Fourier transform, the dynamic structure function $S(\mathbf{k},\tau)$. Figure 8 displays $S(\mathbf{k},\tau)$ of the probe as a function of $k^2\tau$. To improve the signal to noise ratio, $S(\mathbf{k},\tau)$ was obtained by a direct calculation from the particle positions, not by a transform of $P(\delta r,\tau)$. We examined $k \in [0.5, 10.0]$, which covers wavelengths from a small fraction of the lattice spacing $a \approx 3.3$ up to several lattice spacings.

Because the underlying lattice lacks continuous rotational invariance, $S(\mathbf{k},\tau)$ depends on the orientation of $\mathbf{k}$ with respect to the lattice. We therefore obtained $S(\mathbf{k},\tau)$ for three different directions of $\mathbf{k}$, using angles between $\mathbf{k}$ and the x axis of 0°, 22.5°, and 45°. $S(\mathbf{k},\tau)$ was found to

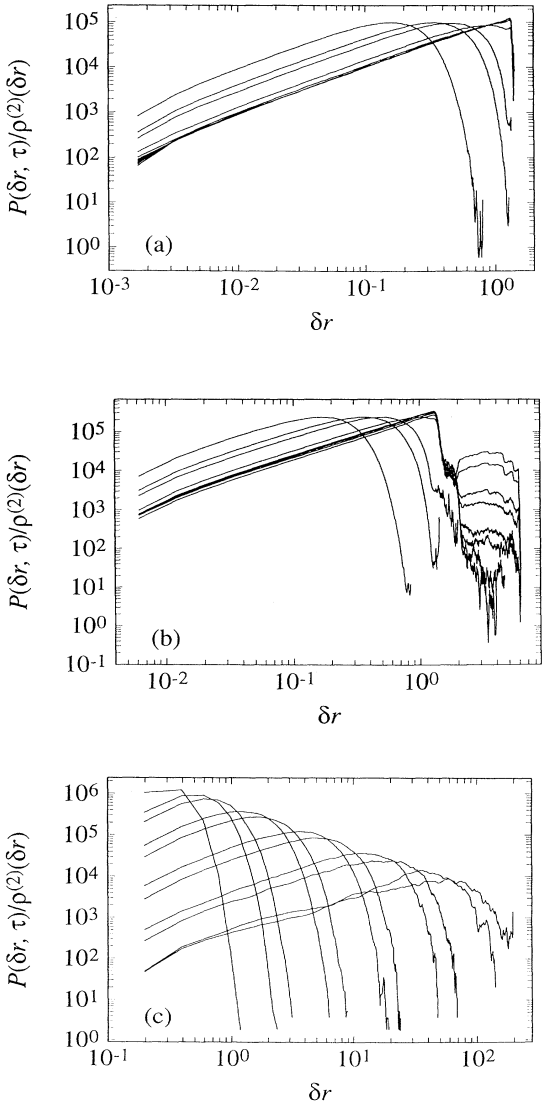

FIG. 7. $\Psi(\delta r,\tau) = P(\delta r,\tau)/\rho^{(2)}(\delta r)$ for the same values of τ used in Fig. 4 at $\rho = 0.09$ and temperatures (a) 0.01, (b) 0.02, and (c) 0.1, showing trapping, hopping, and diffusive behavior, respectively. Some curves were smoothed by averaging over nearby points.

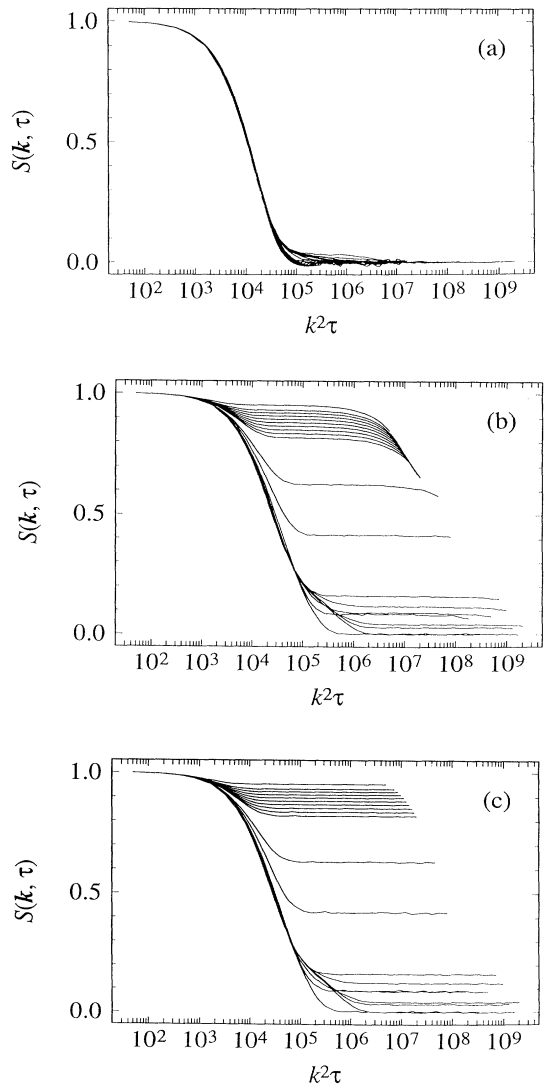

FIG. 8. Dynamic structure function $S(\mathbf{k},\tau)$ of a probe particle as a function of $k^2\tau$ with $\mathbf{k}$ along a lattice line and $\rho = 0.09$, and temperatures $k_B T$ of (a) 0.1 (diffusive behavior), (b) 0.02 (hopping behavior), and (c) 0.01 (trapping behavior).

have a quantitative but not qualitative dependence on the orientation of **k**, so we treat in detail only results for which **k** lies along the lattice axis.

Figure 8(a) describes the high temperature (diffusive) regime. To first approximation $S(\mathbf{k},\tau)$ remains a universal function of $k^2\tau$ even though k^2 varies by 400 fold. This behavior is characteristic of free diffusion, with a diffusion coefficient D renormalized by interactions with the lattice.

At the lower temperature $k_BT=0.02$ [Fig. 8(b), Table II], $S(\mathbf{k},\tau)$ at small k clearly shows decays on two time scales, corresponding to two aspects of probe motion. At short times, motion confined by the potential barrier, i.e., short time trapping, leads to a rapid decay of $S(\mathbf{k},\tau)$. On longer time scales, motion from one lattice site to another, i.e., hopping, completes the relaxation of $S(\mathbf{k},\tau)$. At large k, only motion within the trap can be detected, so only a single diffusion coefficient is obtained (Table II, columns 3 and 4).

Figure 8(c) corresponding to the lowest temperature studied, shows trapping behavior. On short time scales, $S(\mathbf{k},\tau)$ decays to a nonzero constant with a short time diffusion coefficient seen in Table II. $S(\mathbf{k},\tau)$ is approximately constant on longer time scales. Physically, the short time behavior reflects thermalization of the probe position within the trap, while the lack of a long time decay reflects the failure of $\langle[\delta\mathbf{r}(\tau)]^2\rangle$ to increase at large times. The non-zero amplitude of $S(\mathbf{k},\tau)$ for different **k** at large τ corresponds to the spatially nonuniform equilibrium density of the trapped particles.

Table II presents diffusion coefficients obtained by making nonlinear least squares fits to

$$S(\mathbf{k},\tau)=A_1e^{-Dk^2\tau}+B \tag{11}$$

or

$$S(\mathbf{k},\tau)=A_1e^{-D_fk^2\tau}+A_2e^{-D_sk^2\tau}+B\ , \tag{12}$$

where the A_i are amplitudes, the D_i are diffusion coefficients, and B is a baseline; B, the A_i, and the D_i are fitting parameters. $S(\mathbf{k},\tau)$ for trapping, diffusive, and large-k hopping regimes are described by Eq. (11); $S(\mathbf{k},\tau)$ for small-k hopping probes was fitted adequately by Eq. (12). These fits are only approximations; $S(\mathbf{k},\tau)$ is not perfectly exponential at large τ.

TABLE II. Diffusion coefficients found by fitting $S(k,\tau)$ at $\rho=0.09$ and temperatures 0.01 (trapping), 0.02 (hopping), and 0.1 (diffusion) to $A_1\exp(-Dk^2\tau)+B$ or $A_1\exp(-D_fk^2\tau)+A_2\exp(-D_sk^2\tau)+B$, as appropriate. B, A_1, A_2, D, D_f, and D_s are fitting parameters.

	$k_BT=0.01$	$k_BT=0.02$		$k_BT=0.1$
k	D	D_f	D_s	D
0.5	6.29×10^{-4}	6.89×10^{-4}	2.92×10^{-8}	6.28×10^{-5}
0.6	4.38×10^{-4}	4.83×10^{-4}	3.38×10^{-8}	6.36×10^{-5}
0.65	3.73×10^{-4}	4.10×10^{-4}	2.42×10^{-8}	6.41×10^{-5}
0.7	3.22×10^{-4}	3.55×10^{-4}	3.21×10^{-8}	6.47×10^{-5}
0.75	2.81×10^{-4}	3.09×10^{-4}	2.88×10^{-8}	6.52×10^{-5}
0.8	2.47×10^{-4}	2.71×10^{-4}	1.90×10^{-8}	6.56×10^{-5}
0.85	2.19×10^{-4}	2.41×10^{-4}	2.67×10^{-8}	6.59×10^{-5}
0.9	1.96×10^{-4}	2.14×10^{-4}	1.59×10^{-8}	6.63×10^{-5}
0.95	1.76×10^{-4}	1.92×10^{-4}	1.47×10^{-8}	6.66×10^{-5}
1.0	1.59×10^{-4}	1.74×10^{-4}	1.28×10^{-8}	6.69×10^{-5}
1.5	7.30×10^{-5}	7.46×10^{-5}		6.78×10^{-5}
2.0	4.31×10^{-5}	4.72×10^{-5}		6.72×10^{-5}
3.0	2.39×10^{-5}	2.86×10^{-5}		6.86×10^{-5}
4.0	2.41×10^{-5}	3.18×10^{-5}		6.89×10^{-5}
5.0	2.40×10^{-5}	2.82×10^{-5}		6.80×10^{-5}
6.0	2.77×10^{-5}	3.12×10^{-5}		6.67×10^{-5}
7.0	2.33×10^{-5}	2.69×10^{-5}		6.61×10^{-5}
8.0	1.66×10^{-5}	2.56×10^{-5}		6.42×10^{-5}
9.0	1.85×10^{-5}	2.75×10^{-5}		6.10×10^{-5}
10.0	1.29×10^{-5}	1.91×10^{-5}		5.69×10^{-5}

Simple physical considerations explain most of the phenomena seen in Table II. At short times, whether in the trapped, hopping, or diffusive regimes, a particle is able to diffuse more or less freely within a potential energy minimum. Corresponding to this motion, in all systems there is a relatively rapid ($D\sim10^{-4}$) relaxation of $S(\mathbf{k},\tau)$. In a diffusive system [$k_BT=0.1$, Fig. 8(a)], this relaxation persists out to long times with $S(\mathbf{k},\tau)$ going to zero at large τ. In a trapped system [$k_BT=0.01$, Fig. 8(c)], this relaxation persists until the particle has finished exploring its trap; at longer times $S(\mathbf{k},\tau)$ ceases to decay.

In the hopping regime [$k_BT=0.02$, Fig. 8(b)], the behavior of $S(\mathbf{k},\tau)$ is more complicated. At short times, the particle explores its trap, using a "fast" diffusion coefficient D_f little different from the D characteristic of trapped probe particles. At longer times, a hopping particle escapes from its trap. The form of the spectrum hence depends on k. At large k we see primarily short distance motions, so motion of the hopping particle within the trap relaxes $S(\mathbf{k},\tau)$, leading to single exponential decay characterized by D_f. At small k, we see distance over small and over large distances, so both intra- and inter-trap diffusion relax $S(\mathbf{k},\tau)$, leading to a double-exponential decay. With increasing k_BT, the D_f and D_s seen at $k_BT=0.02$ merge into the single decay seen at $k_BT=0.1$. Note that Tables I and II give D/D_0 and D, respectively, so the indicated numbers are not simply comparable.

Figure 9 shows the k dependence of D. At high temperature (triangles), D is seen to have a weak dependence on k, fluctuations of larger wavelength decaying slightly more quickly than fluctuations of lower wavelength. Particles at intermediate and low temperature each show a relaxation corresponding to diffusion within a trapping site; intrasite diffusion coefficients for trapped particles (circles) and hopping particles (squares) are very nearly the same. Finally, hopping particles at low k (corresponding to long distance motions) show a very slow relaxation (diamonds) corresponding to escape from the traps. It is perhaps surprising that this relaxation becomes slower at larger k; we do not attempt a quantitative interpretation of the k dependence of D here. With increasing k_BT, this slow relaxation would be expected to become more rapid, eventually merging with the high temperature free diffusion relaxation (triangles).

At very large k, and all temperatures, D decreases modestly. In this regime kr_0 is not small and the dynamics begin to be affected by the granularity of the random

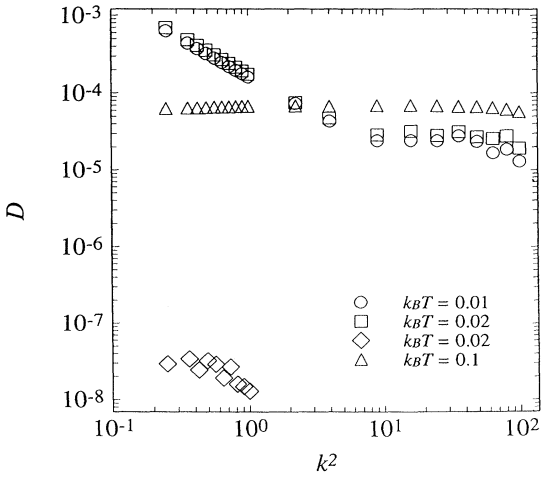

FIG. 9. D from $S(\mathbf{k},\tau)$ of Fig. 8 as a function of k^2 at temperatures 0.1 (open triangles, diffusive behavior), and 0.02 (open squares and diamonds, fast and slow relaxations characteristic of hopping behavior). At $k_BT=0.01$ particles do not diffuse at large times (trapping behavior) and therefore have only apparent short time diffusion coefficients (open circles) that are the same as the short time relaxations seen in the hopping regime.

walk process. The decrease in D at large k can be interpreted as arising from an anticorrelation of successive successful Brownian steps for a particle initially attempting to ascend potential energy surfaces with positive second derivatives.

IV. CONCLUSIONS

We have used Monte Carlo dynamics simulations to study the diffusion of a small probe particle through a square lattice of force centers. The probe-lattice point interaction was the Lennard-Jones potential. Extensive advantage was taken of the ability of computer simulations to determine physical quantities that cannot be measured directly, such as the two-point density of states $\rho^{(2)}(\delta\mathbf{r})$ and the displacement probability density $P(\delta r,\tau)$.

We found a consistent description of all computed functions in terms of a three regime description: (i) trapping, in which particles remain localized on a single lattice site on accessible time scales, (ii) hopping, in which particles are trapped on short time scales but diffuse on longer time scales, and (iii) diffusive, in which $\langle(\delta\mathbf{r})^2\rangle$ increases roughly linearly in time at all observable time scales. The regimes may be identified from the characteristic behaviors of the quantities $\langle[\delta\mathbf{r}(\tau)]^2\rangle$, $P(\delta r,\tau)$, $\Psi(\delta r,\tau)$ and $S(\mathbf{k},\tau)$, and may be understood in terms of the major features of the total potential energy $U(\mathbf{r})$.

In the trapping regime, $P(\delta r,\tau)$ at first broadens with increasing τ and then hits a limit with $P(\delta r,\tau)$ for a trapped particle becoming time independent at sufficiently large times. Corresponding to $P(\delta r,\tau)$, $\langle[\delta\mathbf{r}(\tau)]^2\rangle$ for a trapped particle at first increases linearly in τ and then ceases to increase, while $S(\mathbf{k},\tau)$ decays roughly exponentially in time to a substantially positive plateau value.

In the hopping regime, $\langle[\delta\mathbf{r}(\tau)]^2\rangle$ at first increases linearly with τ, enters a clear plateau region in which the mean-square distance traveled does not change appreciably, and then increases linearly with τ again. This behavior is reflected by a double-exponential decay of $S(\mathbf{k},\tau)$, the fast and slow exponentials corresponding to motion within and between traps, respectively. $P(\delta r,\tau)$ allows one to visualize how trapping and hopping proceed. At short times $P(\delta r,\tau)$ shows a particle that is free to move within some domain, but whose presence beyond the edge of the domain is greatly suppressed. With increasing τ, $P(\delta r,\tau)$ gains an expanding shoulder at larger δr. One sees in $P(\delta r,\tau)$ three spatial regions, namely, an area with the trap, a barrier region within which $P(\delta r,\tau)$ is very small, and a region at larger δr that is gradually populated by particles that have traversed the barrier region. $\Psi(\delta r,\tau)$ reveals that the barrier is caused by phase space rather than dynamic effects; if one divides $P(\delta r,\tau)$ by the two-point density of states $\rho^{(2)}(\delta r)$, the barrier region disappears and $\Psi(\delta r,\tau)$ does not have a deep minimum within the barrier.

Finally, in the diffusive regime, the particle's mean-square displacement increases nearly linearly in time, so that $S(\mathbf{k},\tau)$ is very close to being a universal function of $k^2\tau$ over a factor of 400 in k^2. Correspondingly, $P(\delta r,\tau)$ has a near Gaussian form at all τ, as expected for a diffusing particle.

In both the hopping and diffusive regimes, the probe particle has a well defined effective self-diffusion coefficient $\bar{D}$. $\bar{D}$ is temperature dependent, the dependence being described with reasonable accuracy by an Arrhenius activation energy E_A. E_A is concentration dependent, varying from 0.18 at a density of 0.09 to 0.13 at a density of 0.64.

In the system studied here, trapping occurred in a potential minimum [Fig. 1(a)] having the form of a circular annulus centered on individual particles. The trap may also be seen as a circular annulus in $P(\delta r,\tau)$ [Fig. 5(a)] surrounded by a large area in which $P(\delta r,\tau)$ is virtually zero. At higher potential energies, regions of minimal potential energy change form [Figs. 1(b) and 1(c)], leading to new shapes [Fig. 5(c)] for regions within which particles can be trapped, and between which particles can hop. We explored hopping behavior in the low temperature, high density ($d=0.64$) regime, in which the form of $P(\delta r,\tau)$ [Fig. 5(c)] is very different from its form at low density [Fig. 5(a)], but there are no new qualitative observations apparent from studying this regime.

ACKNOWLEDGMENTS

We wish to thank Nicholas Sushkin for his help in fitting the data in Table II to obtain the diffusion coefficients. L.S.L. and G.D.J.P. would like to acknowledge support by the NSF under Grant No. CHE91-15637 and by the Los Alamos National Laboratory under Grant 9-XA3-4808L. L.C.R. and H.G. would like to thank the Donors of the Petroleum Research Foundation, administered by the American Chemical Society, for partial support of this work.

[1] Y. Guo, J. O'Donahue, K. H. Langley, and F. E. Karasz, Phys. Rev. A **46**, 3335 (1992).
[2] M. T. Bishop, K. H. Langley, and F. E. Karasz, Phys. Rev. Lett. **57**, 1741 (1986).
[3] F. Müller-Plathe, J. Chem. Phys. **94**, 3192 (1991).
[4] I. Nishio, J. C. Reina, and R. Bansil, Phys. Rev. Lett. **59**, 684 (1987).
[5] I. H. Park, C. S. Johnson, Jr., and D. A. Gabriel, Macromolecules **23**, 1548 (1990).
[6] D. B. Sellen, in *Physical Optics of Dynamic Phenomena and Processes in Macromolecular Systems,* edited by B. Sedlacek (de Gruyter, Berlin, 1985), p. 177.
[7] K. Luby-Phelps, S. Mujumdar, R. B. Mujumdar, L. A. Ernst, W. Galbraith, and A. S. Waggoner, Biophys. J. **65**, 236 (1993).
[8] Yu. B. Mel'nichenko, V. V. Klepko, and V. V. Shilov, Europhys. Lett. **13**, 505 (1990).
[9] J. Newman, G. Gukelberger, K. L. Schick, and K. S. Zaner, Biopolymers **31**, 1265 (1991).
[10] Y. Suzuki and I. Nishio, Phys. Rev. B **45**, 4614 (1992).
[11] J. G. H. Joosten, E. T. F. Gelade, and P. N. Pusey, Phys. Rev. A **42**, 2161 (1990).
[12] B. Y. Chen, H. Kim, S. D. Mahanti, T. J. Pinnavaia, and Z. X. Cai, J. Chem. Phys. **100**, 3872 (1994).
[13] L. Hou, F. Lanni, and K. Luby-Phelps, Biophys. J. **58**, 31 (1990).
[14] W. H. Press, S. A. Teukolsky, W. T. Vetterling, and B. P. Flannery, *Numerical Recipes in Fortran,* 2nd ed. (Cambridge University Press, New York, 1992).
[15] N. Metropolis, A. W. Rosenbluth, M. N. Rosenbluth, A. H. Teller, and E. Teller, J. Chem. Phys. **21**, 1087 (1953).
[16] G. H. Vineyard, Phys. Rev. **110**, 999 (1958).